Title

A pilot validation of multi-echo based echo-planar correlated spectroscopic imaging in human calf muscles.

Journal

NMR in biomedicine, 27(10)

ISSN

0952-3480

Authors

Furuyama, Jon K
Nagarajan, Rajakumar
Roberts, Christian K
et al.

Publication Date

2014-10-01

DOI

10.1002/nbm.3171

Peer reviewed

Research article

NMR IN BIOMEDICINE

Received: 3 April 2014, Revised: 11 June 2014, Accepted: 27 June 2014, Published online in Wiley Online Library: 6 August 2014

(wileyonlinelibrary.com) DOI: 10.1002/nbm.3171

A pilot validation of multi-echo based echo-planar correlated spectroscopic imaging in human calf muscles

Jon K. Furuyama[a], Rajakumar Nagarajan[a], Christian K. Roberts[b], Cathy C. Lee[c], Theodore J. Hahn[c] and M. Albert Thomas[a]*

A current limitation of MR spectroscopic imaging of multiple skeletal muscles is prolonged scan duration. A significant reduction in the total scan duration using the echo-planar correlated spectroscopic imaging (EP-COSI) sequence was accomplished using two bipolar readout trains with different phase-encoded echoes for one of two spatial dimensions within a single repetition time (TR). The second bipolar readout was used for spatially encoding the outer *k*-space, whereas the first readout was used for the central *k*-space only. The performance of this novel sequence, called multi-echo based echo-planar correlated spectroscopic imaging (ME-EPCOSI), was demonstrated by localizing specific key features in calf muscles and bone marrow of 11 healthy volunteers and five subjects with type 2 diabetes (T2D). A 3 T MRI–MRS scanner equipped with a transmit–receive extremity coil was used. Localization of the ME-EPCOSI sequence was in good agreement with the earlier single-readout based EP-COSI sequence and the required scan time was reduced by a factor of two. In agreement with an earlier report using single-voxel based 2D MRS, significantly increased unsaturated pools of intramyocellular lipid (IMCL) and extramyocellular lipid (EMCL) and decreased IMCL and EMCL unsaturation indices (UIs) were observed in the soleus and tibialis anterior muscle regions of subjects with T2D compared with healthy controls. In addition, significantly decreased choline content was observed in the soleus of T2D subjects compared with healthy controls. Multi-voxel characterization of IMCL and EMCL ratios and UI in the calf muscle may be useful for the non-invasive assessment of altered lipid metabolism in the pathophysiology of T2D. Copyright © 2014 John Wiley & Sons, Ltd.

Keywords: multi-spin echo, 2D correlated spectroscopy; calf muscle; diabetes; intra-myocellular and extra-myocellular lipids; choline; unsaturation index

INTRODUCTION

Over the past few decades, both MRS and magnetic resonance spectroscopic imaging (MRSI) have evolved as powerful research tools, allowing the study of the underlying biochemistry of various particular tissues (1,2), which can complement standard MRI. Despite their clinical utility, one-dimensional (1D) MR spectroscopic techniques are hindered by overlapping spectral resonances, which can complicate metabolite identification and quantitation. Two-dimensional (2D) spectroscopic techniques have been proposed (3,4) and demonstrated *in vivo* (5–8) to reduce the problem of spectral overlap by spreading resonances into a secondary indirect dimension, improving spectral resolution and peak visibility.

Despite the benefits of 2D spectroscopic techniques, the single-voxel nature of the early techniques limited the spatial coverage, requiring multiple scans to adequately cover multiple locations. The echo-planar spectroscopic imaging (EPSI) sequence employs a repeated readout gradient, simultaneously acquiring one spatial and one spectral dimension in a single repetition time (TR) (9–11). The remaining one spatial dimension in a slice-based 2D EPSI or two spatial dimensions in a volume based three-dimensional (3D) EPSI are subsequently phase encoded, where the desired resolution is proportional to the required scan time.

Recently, the typical EPSI sequence was modified to collect 2D correlated spectroscopy (COSY) data from multiple voxels using an echo-planar correlated spectroscopic imaging (EP-COSI)

* *Correspondence to: M. Albert Thomas, Department of Radiological Sciences, University of California, Los Angeles, CA, USA. E-mail: athomas@mednet.ucla.edu*

a *J. K. Furuyama, R. Nagarajan, M. A. Thomas*
Department of Radiological Sciences, University of California, Los Angeles, CA, USA

b *C. K. Roberts*
Exercise and Metabolic Disease Research Laboratory, Translational Sciences Section, School of Nursing, University of California, Los Angeles, CA, USA

c *C. C. Lee, T. J. Hahn*
Geriatrics, Research, Education and Clinical Center (GRECC), VA Greater Los Angeles Healthcare System, Los Angeles, CA, USA

Abbreviations used: *ME-EPCOSI, multi-echo based echo-planar correlated spectroscopic imaging; IMCL, intramyocellular lipid; EMCL, extramyocellular lipid; T2D, type 2 diabetes; UI, unsaturation index; COSY, correlated spectroscopy; 1D, one-dimensional; 2D, two-dimensional; MRSI, magnetic resonance spectroscopic imaging; EPSI, echo-planar spectroscopic imaging; EP-COSI, echo-planar correlated spectroscopic imaging; VOI, volume of interest; PSF, point-spread function; HbA1c, hemoglobin A1c; WET, water enhanced through T_1 effects; FFT, fast Fourier transform; FOV, field of view; CSI, chemical shift imaging.*

NMR IN BIOMEDICINE

sequence (12). In light of the speed improvements resulting from the EPSI sequence, there have been attempts to further accelerate acquisition. Some attempts include the use of spiral *k*-space trajectories or blipped phase-encoding gradients to cover more *k*-space in a single TR (13–15). Posse and co-workers have used parallel imaging techniques such as SENSE and GRAPPA to reduce the number of excitations (16,17). Recently, a multi-echo based EPSI (ME-EPSI) made use of two spin echoes to collect multiple lines in *k*-space similar to a previous work that employed spin echoes to accelerate the standard MRSI sequence (18–20).

In this study, we propose a modification of the ME-EPSI sequence to collect multi-voxel 2D COSY spectra using a novel multi-echo based echo-planar correlated spectroscopic imaging (ME-EPCOSI) sequence. A two-echo based ME-EPCOSI sequence was tested in calf muscle, and pilot findings in 11 healthy controls and 5 subjects with type 2 diabetes (T2D) are presented here.

THEORY

The ME-EPCOSI sequence is a modified ME-EPSI sequence with two bipolar readout trains as shown in Fig. 1(A). The volume of interest (VOI) was localized using three slice-selective RF pulses similar to those used in point-resolved spectroscopy except that the final 180° pulse is changed to a 90° coherence-transfer pulse (18,21,22). The indirect spectral dimension t_1 is collected by adding an incremental delay (Δt_1) between the first 180° and the final 90° slice-selective RF pulse (6,7,12). Here, a very brief and qualitative description of the coherence transfer process will be provided, while more detailed mathematical formalisms can be found elsewhere (22,23) or in the appendix of a recent study by Lipnick *et al.* (12).

Consider a proton or spin (I) that is weakly J coupled to another spin (S) in the same metabolite. After the initial 90° excitation and 180° refocusing RF pulses, the I spin will evolve according to its own chemical shift (δ_I) and J_{IS}. Following the non-selective coherence transfer 90° pulse, if the I spin is J coupled to the S spin, its coherences will be transferred to the S spin. In other words, the I spin coherences carried in the time before the coherence transfer 90° pulse will be transferred to the other S spin and the coherence will precess according to its own chemical shift (δ_S). The precession of the first spin can be indirectly sampled (t_1) by incrementally sampling the time between the two 90° pulses, whereas the precession on the second spin can be directly sampled (t_2) immediately following the second 90° pulse. A similar transformation happens from the S to I spin before and after the coherence transfer 90° RF pulse. The raw signal is collected as a function of two time variables, $s(t_1, t_2)$. Performing a 2D Fourier transformation on these data will yield a diagonal peak at ($F_2 = F_1$) corresponding to the chemical shift of the first spin (δ_I), and a cross peak at ($F_2 = \delta_I$, $F_1 = \delta_S$). Such peaks in the (F_2, F_1) coordinate system in which $\delta_I \neq \delta_S$ are known as *cross peaks* and indicate that two spins are J coupled, an interaction between spins communicated through covalent bonds. For non-J-coupled resonances, no magnetization can be transferred and so they can be seen at ($\delta_1 = \delta_2$) and are thus referred to as *diagonal peaks*. Unlike 1D MRS sequences in which J-coupled metabolites result in multiplets that can overlap with other resonances, these J-coupled networks can be pushed into a second spectral dimension where they are easier to resolve.

The four-dimensional (4D) EP-COSI sequence samples the second half of the spin-echo created by the VOI localizing pulses, starting at echo time TE_1, and the signal decays due to T_2* relaxation. In contrast, the 4D ME-EPCOSI sequence refocuses the decaying magnetization during the first readout train with a 180° RF pulse and samples a differently phase-encoded *k*-space line as the magnetization grows back until TE_2 during the second readout train within the same TR, as shown in Fig. 1(B). Because of both incoherent T_2 relaxation and coherent J-coupling interaction, the magnetization at TE_2 will not match that at TE_1. Depending on which lines are sampled during the first and second spin echoes, the point-spread function (PSF) will vary. If the *k*-space lines recorded during the second spin echo are placed on the outer edges of *k*-space, the PSF has previously been shown to be as follows (18):

$$h_m(x) = (1 - a)h_h(x) + ah_f(x) \quad [1]$$

where $h_m(x)$ is the multi-echo PSF, $h_h(x)$ is the PSF if only half of the *k*-space is filled (equivalent to the *k*-space lines filled only by the first spin echo), $h_f(x)$ is the PSF if *k*-space is fully sampled with a single spin echo, and a is a reduction factor that represents the change of the magnetization between the beginning of the first readout and the end of the second readout, and can be informally modeled as

$$a = \exp\left\{-\left(\frac{1}{T_2} + i2\pi J\right)\Delta TE_{21}\right\} \quad [2]$$

where $\Delta TE_{21} = TE_2 - TE_1$. Equation [2] is not meant to accurately model the multiplet behavior of J-coupled resonances but rather

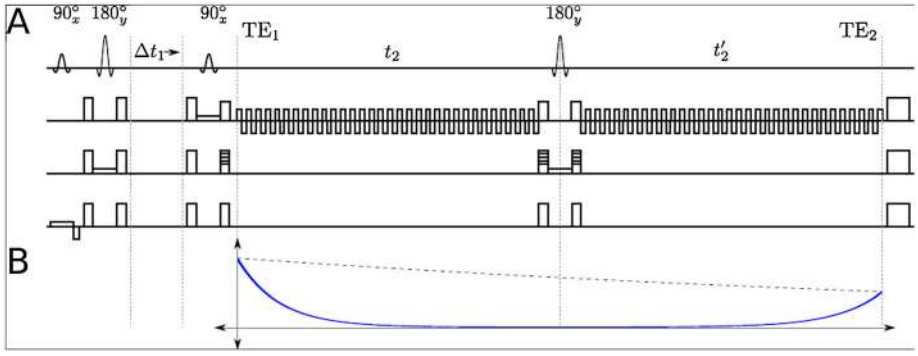

Figure 1. (A) Pulse sequence for a two-echo ME-EPCOSI sequence. The initial phase encoding is combined with the final spoiler before the echo-planar readout. Following the first echo-planar readout (t_2), the initial phase encoding is then reversed just prior to the 180° pulse, to which a different line in *k*-space is phase encoded after the 180° pulse (t_2'). (B) The effect of the spin echo on the actual readout intensity, where the solid line represents the actual observed signal with T_2* decay and the dashed line represents the decay due to irreversible T_2 effects.

to give insight into how the phase of a given peak may be altered at TE_2 due to J coupling.

MATERIALS AND METHODS

Human subjects

The ME-EPCOSI sequence was tested in the calf muscle of 11 healthy volunteers (mean age 32.2 years) and five T2D subjects (mean age 55.2 years). The T2D subjects with a mean hemoglobin A1c (HbA1c) level of 6.0% were well controlled on diet and lifestyle modifications alone, and were not on any medical treatment for diabetes, as determined by medical chart review and confirmation of a documented diagnosis of T2D following performance of a 2 h oral glucose tolerance test. Patients with HbA1c >7.0% were excluded. In addition, subjects with T2D on oral anti-diabetic agents or insulin therapy, or having documented diabetic micro- and macro-angiopathy, were also excluded. Other exclusions included severe renal or hepatic disease, malignancy, or chronic inflammatory diseases such as rheumatoid arthritis. Patients with any contraindications to performing MRI and MRS were also excluded. The 11 healthy volunteers had no history of treatment for T2D, and HbA1c < 5.5%. Written informed consent was obtained from all participants, the project was approved by the UCLA Institutional Review Board, and the study procedures were carried out in accordance with the principles of the Declaration of Helsinki.

Acquisition of MRI and 4D ME-EPCOSI

All scans were performed on a Siemens (Siemens Medical Solutions, Erlangen, Germany) 3 T Trio-TIM MRI scanner running on the VB17a platform and using a single-channel circularly polarized extremity transmit–receive coil. Anatomical MRI included two different MRI scans: a three-plane localizer MRI (TR/TE = 15/5 ms, field of view (FOV) = 45×45 cm^2, 320×160 data matrix, one average) and a T_1 weighted axial spin-echo MRI (TR/TE = 500/2.7 ms, FOV = 16×16 cm^2, 320×256 data matrix, one average).

For the 4D ME-EPCOSI acquisition, a 16×16 cm^2 FOV was localized onto a 16×16 imaging grid and a slice thickness of 2.0 cm for an individual voxel volume of 2.0 cm^3. The measurement parameters for each scan were TR/TE = 1500/30 ms and one average and four preparation excitations to reach a steady-state equilibrium. With an analog-to-digital converter receiver bandwidth of 50 000 Hz and gradient ramp times of 100 μs, the effective dwell time was 840 μs, yielding an F_2 spectral bandwidth of the EPSI readout of 1190 Hz (9.65 ppm). TE_2 in Fig. 1 was 472.5 ms, taking into account that a difference in echo time between the first and second readouts of 442.5 ms. For the indirect spectral dimension, the delay increment was set to $\Delta t_1 = 0.8$ ms, corresponding to an F_1 bandwidth of 1250 Hz (10.14 ppm). Water suppression was performed using a three-pulse water enhanced through T_1 effects (WET) sequence (24), and outer volume suppression bands were applied around the VOI to suppress any signals originating from subcutaneous lipids. In six healthy volunteers, the 4D EP-COSI sequence was also recorded prior to the ME-EPCOSI acquisition for comparison of spatial and spectral quality between the two. Manual B_0 shimming was performed to minimize B_0 inhomogeneity over the localized VOI and the full width at half maximum of the unsuppressed water was typically 15 Hz.

For both the ME-EPCOSI and EP-COSI sequences, 256 bipolar gradient echo pairs were collected for each EPSI readout, yielding 256 t_2 points. 50 t_1 points were incrementally collected resulting in a scan time of 10 min for ME-EPCOSI and 20 min for EP-COSI. For both sequences, a non-water-suppressed scan was acquired using 256 t_2 points, one average with only one t_1 ($\Delta t_1 = 0$) and 16×16 spatial encoding as a reference to correct for eddy current distortions created by the EPSI readout (25). The second reference acquisition took 30 s including four dummy scans to reach the steady state equilibrium.

4D ME-EPCOSI data analysis

All data were extracted and processed according to the flowchart in Fig. 2 using homebuilt MATLAB subroutines. The raw data obtained from the scanner were post-processed using a custom MATLAB-based (MathWorks, Natick, MA, USA) signal processing package. The application of a multi-spin echo sequence with multiple EPSI readout trains requires a few considerations in post-processing. Just as with the EP-COSI sequence,

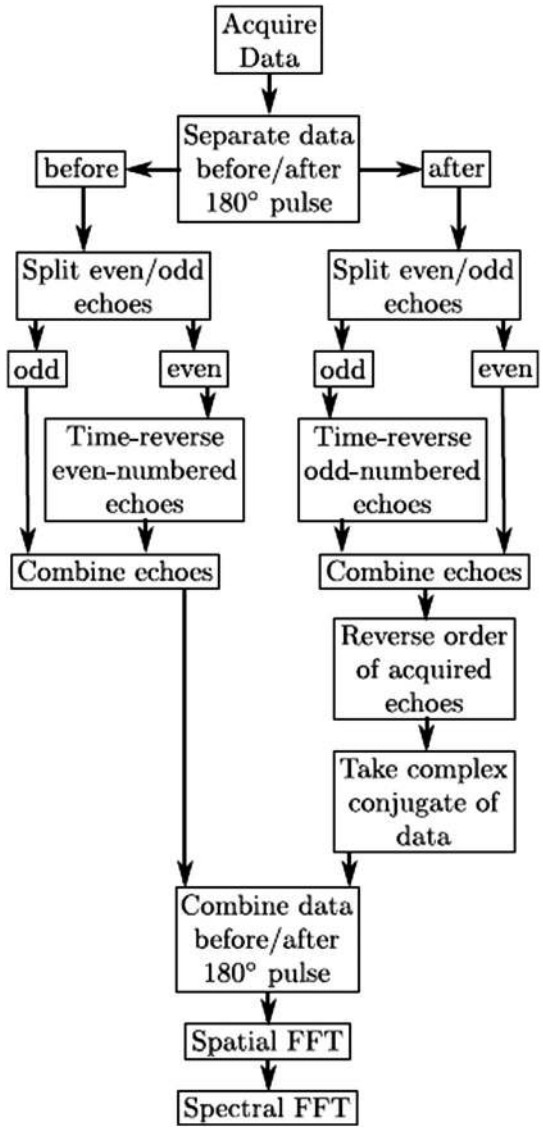

Figure 2. Flowchart of the steps required to process the data acquired from the ME-EPCOSI pulse sequence.

NMR IN BIOMEDICINE

the repeated bipolar readout gradient creates two different sets of *k*-space trajectories that result in mirror images in real space. These two different sets of echoes can be summed together by time-reversing the even-numbered gradient echoes such that the mirror imaging is fixed. The situation changes for the bipolar gradient readout after the spin echo. The first gradient echo after the spin echo corresponds to the last (even-numbered) echo before the spin echo, requiring that all odd-numbered echoes after the spin echo be time reversed.

As can be seen in Fig. 1(B), the maximum amplitude for the first spin echo occurs at the beginning of the EPSI readout (TE_1) whereas the maximum amplitude for the second spin echo occurs at the end of the EPSI readout (TE_2). For proper processing, the order of the second EPSI readout needs to be reversed so that the maximum amplitude occurs at beginning instead of the end. Of course, such a reversal has the effect of mirroring the combined spatial and spectral information of the second EPSI readout, and so the complex conjugate of the second EPSI readout needs to be taken following the reversal. Once all the data are sorted properly, a 2D fast Fourier transform (FFT) can be applied over the spatial dimensions to yield spatially resolved 2D time-domain data.

Raw data retrieved from the scanner were processed in MATLAB through a series of steps including scaling, spatial reordering, phase correction, resolving averages and oversampling (18). Spatial Hamming and skewed sine-bell exponential filters were applied along with eddy current correction in the brain scans to improve overall signal quality (18,25). FFTs were applied twice to the filtered data first along the k_x and k_y dimensions to yield the spatial dimensions *x* (left to right) and *y* (anterior to posterior), respectively. Two more FFTs were applied along the time dimensions t_1 and t_2 to yield the frequency dimensions F_1 and F_2, respectively. The final spectra comprised a 4D matrix arranged in the format $S(F_2, x, y, F_1)$. These spectra were plotted and measured in both MATLAB and the NMR-specific plotting program, Felix-2000 (Felix NMR, San Diego, CA, USA). Using the Felix-2000, the volume integrals of different 2D MRS peaks were calculated as previously described (26,27). Ratios of the volume under each peak (diagonal and cross) were calculated with respect to the diagonal creatine (Cr_d) peak volume at 3 ppm. The cross peak volumes at (IMCL2: 5.3, 2.0 ppm), (IMCL1: 5.3, 2.7 ppm) and (EMCL2: 5.45, 2.15 ppm), (EMCL1: 5.45, 2.85 ppm) were obtained. The degree of unsaturation was estimated by employing these two sets of cross peaks from IMCL2/IMCL1 and EMCL2/EMCL1, designated as the respective unsaturation index (UI) (26–28). This provided a measure of double bonds; i.e., using this ratio the unsaturation within intramyocellular (IMCL) and extramyocellular (EMCL) lipid pools could be assessed.

RESULTS

Figure 3 presents the 4D ME-EPCOSI data acquired from a 27-year-old healthy male volunteer. To confirm the localization, the spatial distribution of the diagonal peak of creatine (N-methylene) at 3.9 ppm is overlaid on top of a T_1 weighted axial spin-echo MRI in Fig. 3(A). The tibial marrow (Fig. 3(B)) mostly contains saturated and unsaturated lipid signals ($(CH_2)_N$, CH_3, CH_2 and CH = CH) and is not expected to show any creatine, water or other metabolite signals. In the tibialis anterior region (Fig. 3(C)), there is a noticeable splitting of the creatine 3.9 ppm peak, which originates from the residual dipolar splitting that has previously been observed in the tibialis anterior (12,29). The residual dipolar coupling of

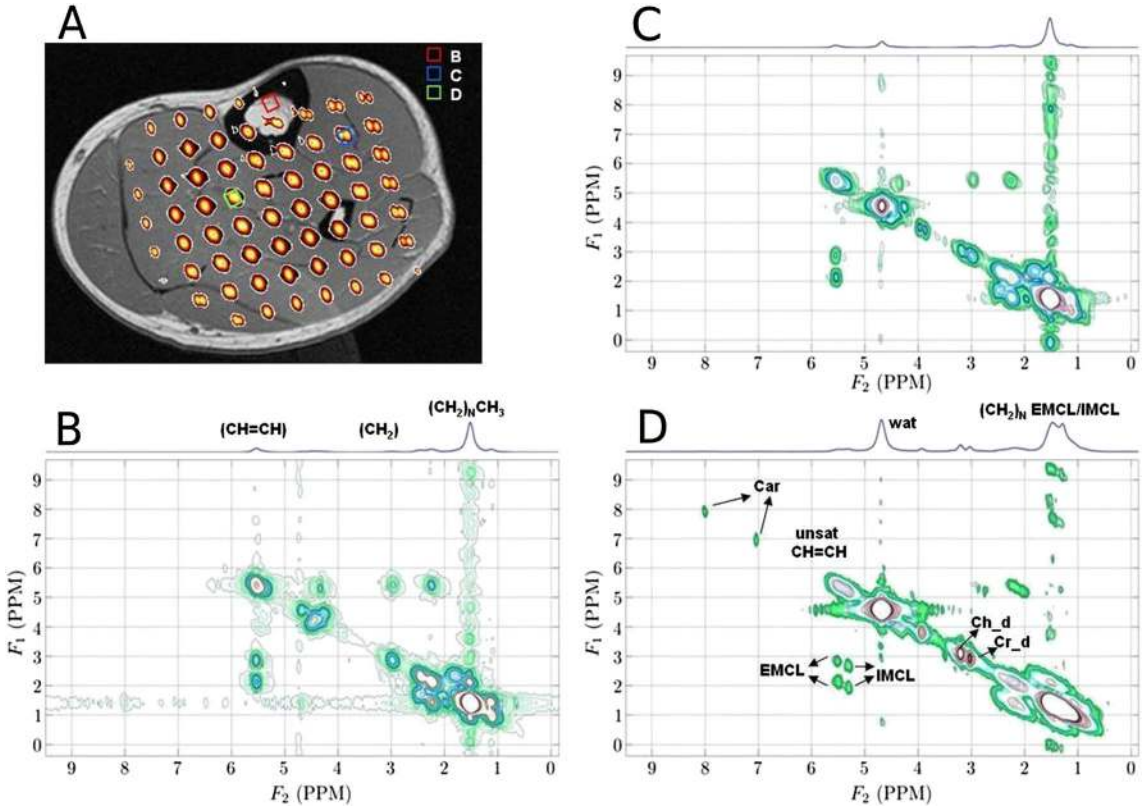

Figure 3. (A) Spatial projection of the creatine 3.9 ppm diagonal peak overlaid on top of T_1 weighted axial MRI in a healthy 27-year-old male volunteer. The 2D spectra along with the 1D projection for specific voxels are taken from (B) the tibial marrow, (C) the tibialis anterior, and (D) the soleus muscle.

creatine is averaged to zero in the soleus muscle (Fig. 3(D)) and thus appears as a singlet on the diagonal.

In the 2D spectra extracted from tibial marrow regions (Fig. 3 (B)), these cross peaks originate from the olefinic protons and methylene protons present in unsaturated fatty acids. In the 1D projection, these two separate peaks show up as only one peak at 5.4 ppm. The 1D peaks at 2.1 ppm and 2.9 ppm are also difficult to resolve, as there is contamination from surrounding peaks, such as the creatine 3.0 ppm peak. In both the 2D spectra extracted from tibialis anterior (Fig. 3(C)), there are two cross peaks at (5.4, 2.9) ppm and (5.4, 2.1) ppm, originating from the olefinic protons present in unsaturated fatty acids, which are termed extramyocellular lipids (EMCL) and intramyocellular lipids (IMCL). In the soleus muscle (Fig. 3D), the olefinic cross peaks are known to split due to the presence of EMCL as well as IMCL. It can be seen that the splitting due to the EMCL/IMCL is much easier to resolve in the cross peaks as opposed to the dominant lipid signal on the diagonal around 1.4 ppm, which suffers from severe spectral overlap. Figure 3(D) also shows the presence of carnosine peaks at 7 ppm and 8 ppm which are very weak in the 1D projection but shows up quite nicely in the 2D spectrum as reported earlier using the single-voxel based L-COSY (26,27).

Figure 4 shows the spatial distribution of the creatine 3.9 ppm peak for both data acquired using the ME-EPCOSI (A) as well as the EP-COSI sequences (B) from a 28-year-old volunteer. It can be seen that both sequences yield very similar spatial distributions of the creatine 3.9 ppm peak despite the added T_2 weighting during the second EPI-train readouts. Absolute peak volumes of selected 2D diagonal (Ch_d, $(CH_2)_N$) and 2D cross peaks (IMCL1 and EMCL1) resonating at the following locations were quantified: ($F_2 = F_1 = 3.15$ ppm), ($F_2 = F_1 = 1.3$ ppm), ($F_2 = 5.3$ ppm, $F_1 = 2.7$ ppm), ($F_2 = 5.45$ ppm, $F_1 = 2.85$ ppm) in the EP-COSI and ME-EPCOSI data recorded in soleus and tibialis anterior muscle regions of six healthy volunteers. A correlation analysis was done using the above mentioned 2D diagonal and cross peak ratios recorded using the EP-COSI and ME-EPCOSI data. A positive correlation was observed in the 2D diagonal peak volumes of Ch/Cr_d, polymethylene (CH_2)N/Cr_d and cross peaks of EMCL1/Cr and IMCL1/Cr in soleus and tibialis anterior regions of six healthy subjects. The R^2 values of diagonal peaks ranged between 0.81 and 0.96 in both soleus and tibialis anterior muscles of six healthy subjects. Similarly analyzing the cross peaks of EMCL and IMCL, the R^2 values were between 0.583 and 0.915 in the soleus and tibialis anterior locations of six healthy subjects.

Figure 5 shows a select ME-EPCOSI spectrum taken from the tibialis anterior region of a 57-year-old subject with T2D. The location of the voxel as shown in the inset of Fig. 5 is confirmed, as the creatine 3.9 ppm diagonal peak can be seen to be split. Unlike the tibialis anterior in the healthy volunteers, there is a clear presence of IMCL in addition to the expected EMCL. As can be seen in the 1D projection, the splitting of the EMCL and IMCL is difficult to resolve at 1.4 ppm due to the severe spectral overlap. Shown in Table 1 are IMCL/Cr and EMCL/Cr ratios and UI of IMCL and EMCL recorded in the soleus and tibialis anterior regions of 5 T2D patients and 11 healthy subjects. As shown in Table 1, T2D patients exhibited significantly elevated IMCL/Cr ratios in both the soleus and tibialis anterior regions compared with healthy controls ($p < 0.05$). Non-significant changes in UI of IMCL in the soleus and tibialis anterior regions of T2D patients compared with healthy controls are also presented. Table 1 also shows the following: (1) significantly elevated EMCL/Cr ratios in the soleus and tibialis anterior regions in T2D patients compared with healthy controls ($p < 0.05$) and (2) significantly elevated EMCL UI in the soleus muscle, with a similar trend observed in tibialis anterior. Shown in Table 2 is the regional variation of significantly decreased choline to creatine ratios in the soleus muscle and a similar trend observed in tibialis anterior.

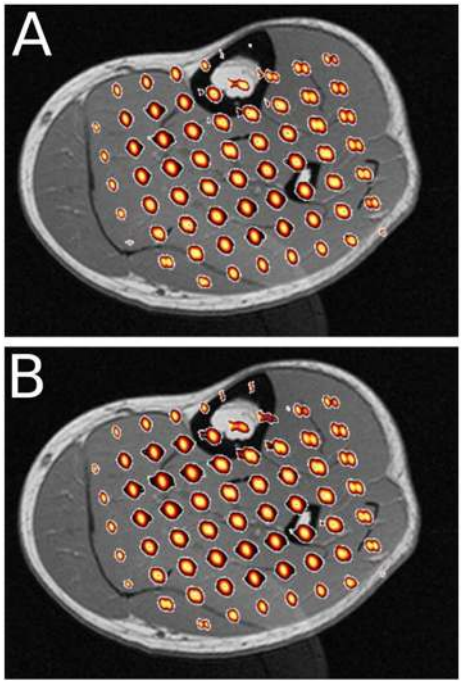

Figure 4. Spatial projection of the creatine 3.9 ppm diagonal peak in a healthy 28-year-old male volunteer overlaid on top of T_1 weighted axial MRI, comparing the performance of the (A) ME-EPCOSI sequence and the (B) EP-COSI sequence.

DISCUSSION

Using two EPI-readout trains sandwiched by a refocusing 180° RF pulse, the present study demonstrates that the acquisition time of the standard 4D EP-COSI sequence can be reduced by half while maintaining sufficient spectral and spatial quality. While

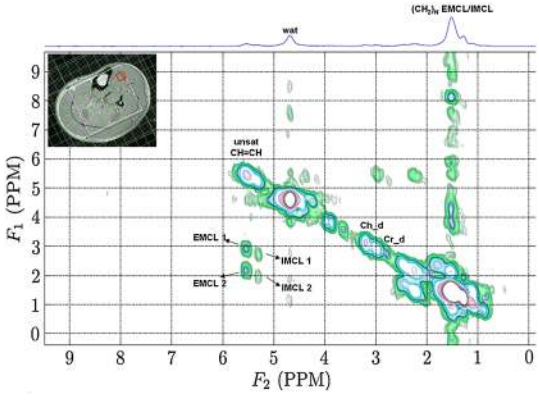

Figure 5. An extracted 2D spectrum of the tibialis anterior acquired using the ME-EPCOSI sequence in a 57-year-old subject with T2D with an MRI localizer (inset) showing the voxel used for the ME-EPCOSI sequence. The location of the tibialis anterior is verified by the splitting of the creatine 3.9 ppm peak due to the residual dipolar coupling.

NMR IN BIOMEDICINE

Table 1. Ratios of IMCL and EMCL (/Cr), and UI values in the soleus muscle and tibialis anterior regions

Location	Subject group	EMCL/Cr	IMCL/Cr	UI for EMCL	UI for IMCL
Soleus muscle	diabetes	0.31 ± 0.07*	0.09 ± 0.03*	0.89 ± 0.13*	0.80 ± 0.11
	healthy	0.11 ± 0.06	0.05 ± 0.02	0.70 ± 0.14	1.00 ± 0.13
Tibialis anterior	diabetes	0.50 ± 0.12*	0.08 ± 0.10*	0.95 ± 0.15	1.00 ± 0.12
	healthy	0.37 ± 0.11	0.05 ± 0.13	0.82 ± 0.14	1.02 ± 0.16

*$p < 0.05$ between diabetic and healthy subjects.

Table 2. Choline ratios (with respect to Cr) in different muscles

Subject groups	Soleus muscle	Tibialis anterior
Diabetic	0.68 ± 0.11*	0.53 ± 0.42
Healthy	1.03 ± 0.18	0.67 ± 0.19

*$p < 0.05$ between diabetic and healthy subjects.

this study only employed two spin echoes, additional echoes can be used provided the signal has not sufficiently decayed due to T_2 effects. The use of multiple spin echoes within a single TR is equivalent to filling *k*-space with different TE values. In the absence of T_2 relaxation and *J* coupling, the ME-EPSI sequence (or other multi-spin-echo sequences) can improve the spatial resolution of standard chemical shift imaging (CSI) sequences without any artifacts. Both T_2 relaxation and *J* evolution originate from terms in the Hamiltonian that are not refocused by a 180° pulse, resulting in an amplitude and phase modulation in the *k*-space encoding that can lead directly to both spectral and spatial Gibbs ringing in the data. More discussion can be found in the earlier work (18).

In this pilot study involving 5 T2D and 11 healthy subjects, the coefficients of variance of UI of IMCL and EMCL, and the IMCL/Cr and EMCL/Cr ratios, were below 20%. The changes in IMCL and EMCL ratios and UIs recorded using the 4D ME-EPCOSI sequence were in good agreement with the single-voxel based L-COSY study with the capability of detecting multiple-voxel 2D COSY spectra in one recording (26–28). A new finding emerging from this study includes significantly decreased choline in the soleus muscle of T2D subjects compared with healthy subjects.

The spatial distribution of the creatine 3.9 ppm peak in Fig. 3 (A) shows that the ME-EPCOSI sequence correctly encodes each voxel based in the expected anatomy. In the voxels surrounding the tibial marrow, the creatine 3.9 ppm peak can be seen to almost completely disappear as creatine, is not known to exist in bone marrow. It can be seen in both Figs. 3 and 4 that the creatine 3.9 ppm signal was seen in some of the voxels that include the marrow. This might first be mistaken to be a consequence of spatial distortions that are to be expected from the use of spin echoes, but, as can be seen in comparing EP-COSI with ME-EPCOSI, the same feature shows up despite the lack of spin echoes in EP-COSI. Consequently, the bleeding of the creatine 3.9 ppm peak into marrow voxels is likely to be the result of a chemical shift artifact instead of a limitation of the multi-echo sequence. As is the case with all CSI-based sequences, these chemical shift artifacts can be reduced with the implementation of stronger slice-selection gradients. Despite the signal bleed of creatine into the marrow voxels, the concentration is hardly noticeable compared with the high-concentration lipid signals present in bone marrow. The cross peaks originating from the olefinic protons in poly- and mono-unsaturated fats can be clearly seen at (5.4, 2.9) ppm and (5.4, 2.2) ppm.

The appearance of the olefinic cross peaks changes in the soleus muscle due to the presence of both EMCL as well as IMCL. EMCLs are lipids that are typically found in all muscles. Recently there has been a growing interest in the study of IMCLs in skeletal muscle, as their concentrations are highly variable depending on metabolism, health status and exercise training status. IMCLs are small intracellular lipid droplets within muscle, and these fat signals have a slightly altered chemical shift from the EMCL signals, as can be seen in Fig. 3(D). The IMCL droplets do not shift the resonances. However, the EMCL plates shift the resonances away from their original chemical shifts due to susceptibility effects. As a result of the primary dependency of muscle on fat as a fuel source, the IMCLs are generally higher in the soleus, with its greater percentage of type I muscle fibers. The tibialis anterior, with greater type II fiber makeup, is generally characterized as having lower IMCL content. As can be seen in Fig. 3(D), the IMCL peaks appear with the same intensity as the EMCL peaks. The most likely explanation lies in the physical differences between EMCL and IMCL. The droplet nature of the IMCL allows for greater molecular mobility, leading to an increased T_2 relaxation time (30). The T_2 weighting introduced by the use of spin echoes would thus have a more detrimental effect on species such as EMCL that have shorter T_2 times leaving signals from IMCL to be brighter than in an ordinary EP-COSI sequence without added T_2 weighting.

The levels of IMCL in the tibialis anterior muscle of the T2D subjects as shown in Table 1 may be a marker for altered metabolic status, where insulin resistance is associated with altered lipid metabolism, and in endurance trained subjects where the tibialis anterior IMCL content is paradoxically elevated (31), commonly referred to as the athletes' paradox. An example of the increased IMCL in the tibialis anterior is depicted in Table 1, where this voxel is from the tibialis anterior, due to the splitting of the creatine 3.9 ppm peak. In contrast to Fig. 3(C), the presence of more intense olefinic cross peaks can be seen in Fig. 5. This observation is the same as that made with the EP-COSI sequence in endurance trained athletes (12). The 4D ME-EPCOSI sequence can thus be seen to properly localize different muscle fiber types, while also being sensitive to different metabolic patterns inherent to muscle of variable fiber types in different tissues.

Table 2 shows our first time demonstration of regional variation and significantly decreased choline (also known as trimethylamine, TMA) ratios in T2D subjects compared with healthy controls. It has been also shown that the TMA resonance contains carnitine and acetylcarnitine, and both molecules play critical roles in muscle metabolism (32,33). It should be noted that a limitation of our

current small pilot study is the inability to attribute the observed differences in myocellular lipids and choline ratios between groups solely to T2D per se, exclusive of other differences between the two groups, including age, BMI, physical activity levels, diet and/or hormonal status. More definitive answers in this regard must await future larger controlled studies.

Though the 4D ME-EPCOSI sequence is shown to have very similar performance compared with its non-spin-echo-based counterpart, some concerns will need to be addressed specifically for quantitation purposes. Two avenues for quantitation errors arise in the use of spin echoes, since the inner phase-encoded *k*-space lines have a shorter effective TE than the *k*-space lines on the periphery. Since a spin echo does not reverse the action of either T_2 decay or *J* evolution, there are expected distortions, as different lines in *k*-space will contain different spectroscopic information. From a qualitative as well as a quantitative perspective, the ME-EPCOSI sequence has comparable performance to the EP-COSI sequence. All anatomical features are correctly spatially encoded, as can be seen in comparing the different spectral features in the tibialis anterior, the tibial marrow and the soleus. Cross peak signals are *J* modulated by definition, but show no serious degradation due to the use of spin echoes. For the sake of quantitation purposes, a further analysis on the effect of mixing *k*-space lines at different *TE* values is needed and will be presented in a future work. At the expense of F_2 spectral resolution, the number of collected t_2 points can be reduced to in order to minimize any differences originating from the different TE values.

CONCLUSION

We have shown that the implementation of the two-echo based ME-EPCOSI sequence has performance similar to that of the regular EP-COSI sequence with only half of the acquisition time. The spatial and spectral performance was tested *in vivo* and yields accurate anatomical information, specifically in the tibial marrow and both tibialis anterior and soleus muscles. The added T_2 decay and *J* evolution introduced into the outer *k*-space lines from the spin-echo did not appear to degrade the image quality despite the typically shorter T_2 values found in the calf muscle. Even with the lower spectral resolution compared with the EP-COSI technique, the ME-EPCOSI still succeeded in being able to resolve the cross peaks from the EMCL/IMCL, as evident from our pilot findings of correlating selected 2D diagonal and cross peaks from the ME-EPCOSI and EP-COSI data. The benefits of 2D spectroscopy *in vivo* have been previously demonstrated in its ability to resolve a greater number of spectral resonances resulting from the increased spectral dispersion in the second dimension. The greatest obstacle to the widespread use of the L-COSY technique *in vivo* has been its limited spatial coverage, as well as the amount of time required for scanning. With the ME-EPCOSI sequence, multiple 2D COSY spectra can be measured in a 10 min scan across a plane with voxel volumes of 2 cm^3 (1 cm × 1 cm × 2 cm) compared with the usual single 27 cm^3 (3 cm × 3 cm × 3 cm) voxel. Thus, with this reasonable scan duration, it is demonstrated here that the ME-EPCOSI is an innovative method for *in vivo* studies of muscle lipid content in T2D and a variety of other metabolic conditions, as well as in response to interventions. Furthermore, the ME-EPCOSI technique may be further accelerated through the implementation of parallel imaging techniques, having the benefit of quicker scan times or higher imaging resolution.

Acknowledgements

The authors acknowledge the support of Dr Preethi Srikanthan during an earlier phase of this project.

This work was partially funded by an NIH/NIDDK grant (5R01DK090406).

Presented at the 21st ISMRM Meeting, Salt Lake City, UT, April 20–26, 2013.

REFERENCES

1 Lin AP, Liao HJ, Merugumala SK, Prabhu SP, Meehan WP 3rd, Ross BD. Metabolic imaging of mild traumatic brain injury. Brain Imaging Behav. 2012; 6: 208–223.
2 Bittsansky M, Vybohova D, Debrota D. Proton magnetic resonance spectroscopy and its diagnostically important metabolites in the brain. Gen. Physiol. Biophys. 2012; 31(1): 101–112.
3 Jeener J. *Ampere International Summer School, Basko Polje, Yugoslavia*, 1971.
4 Aue W, Bartholdi E, Ernst R. Two-dimensional spectroscopy. Application to nuclear magnetic resonance. J. Chem. Phys. 1976; 64: 2229–2246.
5 Ryner L, Sorenson J, Thomas M. Localized 2D *J*-Resolved ^{1}H MR spectroscopy: strong coupling effects in vitro and in vivo. Magn. Reson. Imaging 1995; 13: 853–869.
6 Thomas MA, Yue K, Binesh N, Davanzo P, Kumar A, Siegel B, Frye M, Curran J, Lufkin R, Martin P, Guze B. Localized two-dimensional shift correlated MR spectroscopy of human brain. Magn. Reson. Med. 2001; 46: 58–67.
7 Thomas MA, Hattori N, Umeda M, Sawada T, Naruse S. Adding a new spectral dimension to localized 3 T 1H MR spectroscopy – from phantoms to human brain in vivo. NMR Biomed. 2003; 16: 245–251.
8 Thomas MA, Nagarajan R, Huda A, Margolis D, Sarma MK, Sheng K, Reiter RE, Raman SS. Multidimensional MR spectroscopic imaging of prostate cancer in vivo. NMR Biomed.. 2014; 27(1): 53–66.
9 Mansfield P. Spatial mapping of the chemical shift in NMR. J. Phys. D Appl. Phys. 1983; 16: L235–L238.
10 Posse S, DeCarli C, Le Bihan D. Three-dimensional echo-planar MR spectroscopic imaging at short echo times in the human brain. Radiology 1994; 192(3): 733–738.
11 Ebel A, Maudsley AA, Schuff N. Correction of local B0 shifts in 3D EPSI of the human brain at 4 T. Magn. Reson. Imaging 2007; 25: 377–380.
12 Lipnick S, Verma G, Ramadan S, Furuyama J, Thomas MA. Echo planar correlated spectroscopic imaging: implementation and pilot evaluation in human calf in vivo. Magn. Reson. Med. 2010; 64: 947–956.
13 Mulkern R, Panych L. Echo planar spectroscopic imaging. Concepts Magn. Reson. 2001; 13: 213–237.
14 Adalsteinsson E, Irarrazabal P, Spielman D, Macovski A. Three-dimensional spectroscopic imaging with time varying gradients. Magn. Reson. Med. 1995; 33: 461–466.
15 Webb P, Spielman D, Macovski A. A fast spectroscopic imaging method using a blipped phase encode gradient. Magn. Reson. Med. 1989; 12: 306–215.
16 Lin F, Tsai S, Otazo R, Caprihan A, Wald L, Belliveau J, Posse S. Sensitivity-encoded (SENSE) proton-echo-planar-spectroscopic imaging (PEPSI) in human brain. Magn. Reson. Med. 2007; 57: 249–257.
17 Tsai S, Posse S, Otazo R, Lin Y, Chung H, Lin F. Accelerated proton–echo-planar spectroscopy imaging (PEPSI) using GRAPPA with large-N phased-array coils. Magn. Reson. Med. 2008; 59: 989–998.
18 Furuyama J, Burns B, Wilson N, Thomas MA. Multi-echo-based echo-planar spectroscopic imaging using a 3 T MRI scanner. Materials 2011; 4: 1818–1834.
19 Duyn J, Moonen C. Fast proton spectroscopic imaging of human brain using multiple spin-echoes. Magn. Reson. Med. 1993; 30: 409–414.
20 Dreher W, Leibfritz D. Fast proton spectroscopic imaging with high signal-to-noise ratio: spectroscopic RARE. Magn. Reson. Med. 2002; 47: 523–528.
21 Bottomley P. Spatial localization in NMR spectroscopy in vivo. Ann. N. Y. Acad. Sci. 1987; 333–348.
22 Ernst RR, Bodenhausen G, Wokaun A. *Principles of Nuclear Magnetic Resonance in One and Two Dimensions*. Clarendon Press: Oxford, UK; 1987.

23 Levitt M. Spin Dynamics. Basics of Nuclear Magnetic Resonance. Wiley: Chichester, United Kingdom; 2001.
24 Ogg R, Kingsley P, Taylor J. WET, a T_1- and B_1-insensitive water-suppression method for *in vivo* localized ^{1}H NMR spectroscopy. J. Magn. Reson. B 1994; 104: 1–10.
25 Klose U. In vivo proton spectroscopy in presence of eddy currents. Magn. Reson. Med. 1990; 14: 26–30.
26 Velan SS, Said N, Durst C, Frisbee S, Frisbee J, Raylman RR, Thomas MA, Rajendran VM, Spencer RG, Alway SE. Distinct patterns of fat metabolism in skeletal muscle of normal-weight, overweight, and obese humans. Am. J. Physiol. Regul. Integr. Comp. Physiol. 2008; 295(4): R1060–R1065.
27 Velan SS, Durst C, Lemieux SK, Raylman RR, Sridhar R, Spencer RG, Hobbs GR, Thomas MA. Investigation of muscle lipid metabolism by localized one- and two-dimensional MRS techniques using a clinical 3 T MRI/MRS scanner. J. Magn. Reson. Imaging 2007; 25: 192–199.
28 Srikanthan P, Singhal A, Lee CC, Nagarajan R, Wilson N, Roberts CK, Hahn TJ, Thomas MA. Characterization of intra-myocellular lipids using 2D localized correlated spectroscopy and abdominal fat using MRI in type 2 diabetes. Magn. Reson. Insights 2012 (Oct. 15); 5: 29–36.
29 Kreis R, Boesch C. Liquid-crystal-like structures of human muscle demonstrated by in vivo observation of direct dipolar couplings in localized proton magnetic resonance spectroscopy. J. Magn. Reson. B 1994; 104: 189–192.
30 Krssak M, Mlynarik V, Meyerspeer M, Moser E, Roden M. ^{1}H NMR relaxation times of skeletal muscle metabolites at 3 T. Magn. Reson. Mater. Phys. Biol. Med. 2004; 16: 155–159.
31 Boesch C, Machann J, Vermathen P, Schick F. Role of proton MR for the study of muscle lipid metabolism. NMR Biomed. 2006; 19: 968–988.
32 Boss A, Kreis R, Saillen P, Zehnder M, Boesch C, Vermathen P. Skeletal muscle ^{1}H MRSI before and after prolonged exercise. II. Visibility of free carnitine. Magn. Reson. Med. 2012; 68(5): 1368–1375.
33 Ren J, Lakoski S, Haller RG, Sherry AD, Malloy CR. Dynamic monitoring of carnitine and acetylcarnitine in the trimethylamine signal after exercise in human skeletal muscle by 7 T ^{1}H-MRS. Magn. Reson. Med. 2013; 69(1): 7–17.

